Hindawi Publishing Corporation
Journal of Nanomaterials
Volume 2016, Article ID 1805169, 15 pages
http://dx.doi.org/10.1155/2016/1805169

Research Article

Influence of Phases Content on Pt/TiO_2, Pd/TiO_2 Catalysts for Degradation of 4-Chlorophenol at Room Temperature

D. S. García-Zaleta,[1,2] A. M. Torres-Huerta,[1] M. A. Domínguez-Crespo,[1] A. García-Murillo,[3] R. Silva-Rodrigo,[4] and R. López González[5]

[1]*CICATA Altamira, Instituto Politécnico Nacional, Km 14.5, Carretera Tampico-Puerto Industrial Altamira, 89600 Altamira, TAMPS, Mexico*
[2]*División Académica Multidisciplinaria de Jalpa de Méndez, Universidad Juárez Autónoma de Tabasco, Carretera Estatal Libre VHS-COM Km 27+000 s/n Ranch. Ribera Alta, 86205 Jalpa de Méndez, TAB, Mexico*
[3]*CIITEC, Instituto Politécnico Nacional, Cerrada de Cecati s/n, Colonia Santa Catarina, 02250 Azcapotzalco, DF, Mexico*
[4]*Instituto Tecnológico de Ciudad Madero, Avenida Primero de Mayo s/n, Colonia Los Mangos, 89440 Ciudad Madero, TAMPS, Mexico*
[5]*Division Académica de Ingeniería y Arquitectura, Universidad Juarez Autónoma de Tabasco (UJAT-CICTAT), Carretera Cunduacan-Jalpa Km 1, Colonia La Esmeralda, 86690 Cunduacán, TAB, Mexico*

Correspondence should be addressed to D. S. García-Zaleta; davidsalvador79@hotmail.com

Received 22 February 2016; Revised 30 April 2016; Accepted 9 May 2016

Academic Editor: Jim Low

Different Pt/TiO_2 and Pd/TiO_2 catalysts were prepared by sol-gel method. The influence of different amounts of noble metals (1–5 mol-%) present on the microstructure as well as the photocatalytic property under 4-chlorophenol degradation was evaluated. The anatase phase was favored at low Pt content; however, the apparition of new phases after 3 mol-% (PtO) suggests a saturation lattice considering our solubility limit at 1 mol-%. Similar trend was observed when Pd was added to the TiO_2 lattice. The as-prepared catalysts were deeply characterized by X-ray diffraction (XRD) with the Rietveld Method, Raman spectroscopy, high resolution scanning electron microscopy (HRSEM), scanning transmission electron microscopy (STEM), Brunauer-Emmett-Teller (BET) adsorption analysis, and X-Ray photoelectron spectroscopy (XPS). Unit-cell parameter of TiO_2 phases varied from 30 to 93 vol-% depending on the amount of Pt or Pd added to the composite. HRTEM and HRSEM identified the phases in the catalysts and confirmed the nanometric size and morphology of the catalysts. An improvement in removal efficiency of 4-chlorophenol was obtained in all the specimens compared with the commercial Degussa P25, which can be explained in terms of phase composition and modification of the band gap.

1. Introduction

The current world population growth has provoked a big pollution problem for the overexploitation of natural resources and continuous use of toxic substances applied in the production of many materials. In this way, chlorophenols (CPs) are extensively used in the synthesis of pesticides, herbicides, and dyes and as preservative agents for wood, paints, fibers, and leather [1]. Most of the CPs have been listed as priority pollutants due their acute toxicity, resistance to biodegradability, and strong bioaccumulation potential [2]. Therefore, removal or degradation of hazardous materials and contaminants from wastewater, ground, or surface water is a significant global challenge; many methods including biological, chemical, or physical methods have been developed to make the water free of toxic chemicals and pathogens [3].

The use of semiconductors as photocatalysts has emerged as promising method in the area of catalysis [4]. Among the semiconductors used, titanium dioxide (TiO_2) is one of the most suitable material due to it showing four crystal structures: anatase, rutile, brookite, and $TiO_2(\beta)$ [5, 6]. The functional properties depend on the phase and combining them could achieve synergic effects [7, 8]. In addition, TiO_2 shows high photocatalytic activity, good photostability,

nontoxicity, and low price. However, its main drawbacks in effective commercial applications are the agglomeration of ultrafine powders, which prompt an adverse effect on the catalyst performance as well as its band gap (3.2 eV) that avoids the use of sunlight [9]. In this way, many strategies have been developed to overcome these limitations, such as synthesis of compounds with crystal phase combinations [10–12] and noble metal doping [4, 9]. Also, some researches have reported the effect of tridoped and quaternary doped in anatase-TiO_2 nanophotocatalysts [13, 14].

It has been showed that the incorporation of noble metals (Ag, Ni, Cu, Au, Rh, Pt, and Pd) [9, 15] into the TiO_2 lattice improves the photocatalytic properties of this compound. Pt and Pd ions have shown excellent efficiency in diverse applications, such as hydrogenation of aromatic hydrocarbons, electrooxidation of small organic molecules with high sulfur [16], CO reduction [17], and in the degradation of several contaminants [18]. On the other hand, it is important to consider the preparation procedures as well as the optimal conditions to achieve high quality catalyst. So far, the sol-gel method has demonstrated to be an effective technique for the TiO_2 lattice ion incorporation [16]. Our previous report has evidenced that at 400°C the addition of different Pd amounts can modulate the photocatalytic performance of the Pd-doped TiO_2 materials [19]. The present study was thus undertaken in order to investigate the structure and catalytic performance of Pt-doped TiO_2 composites and compared with the Pd-doped TiO_2 at 500°C. The effect of phase composition with temperature was also analyzed. The conditions used during the catalysts synthesis favored the incorporation of the noble metals into the anatase lattice and the different amounts of noble metal allowed obtaining diverse percentages of anatase and rutile mainly. The photocatalytic activity of the compounds was evaluated in the degradation of 4-chlorophenol under UV light.

2. Materials and Methods

2.1. Catalysts Preparation. In this paper the noble metals doped titania were prepare for the sol-gel synthesis using as precursors titanium isopropoxide ($Ti[OCH(CH_3)_2]_4$, 97.0%), palladium acetylacetonate ($Pd(C_5H_7O_2)_2$, 99.0%), platinum acetylacetonate ($Pt(C_5H_7O_2)_2$, 97.0%), isopropanol ($(CH_3)_2CHOH$, 99.9%), methanol (CH_3OH, 99.9%), and acetic acid (CH_3COOH, 99.9%), which were procured from Sigma Aldrich, Fluka, and J. T. Baker and used without any pretreatment. The Xerogels were prepared by previously reported sol-gel process using mixing stoichiometric amounts of the different precursors in acid media to obtain composites of platinum or palladium doped TiO_2 with a molar ratio of 1, 3, and 5 [19]. Thereafter, as-obtained samples were thermally treated at 500°C with a ramp of 7°C per minute followed by a milling process to homogenize the particle size.

2.2. Characterization Methods. Powder XRD data for the thermal treated samples were acquired on a Bruker D8 advance machine with a Cu Kα radiation and equipped with a Linxeye detector. Data were collected in the 2θ range 20–100° with a step size of 0.017° and a step time of 21.4 s. Rietveld refinement was performed for further analysis using *TOPAS 3.0* software and the representation of the refined structures was realized by the Crystalmaker 2.5 software. Phase characterization was also realized by Raman spectra measurements using a Spex 1043 double monochromator (Edison, New Jersey) with 514.5 nm line of argon laser (lexel laser) at a power level of 40 mW (800–100 cm^{-1}). Morphological features of the as-prepared samples were observed with the scanning electron microscopes (FEI QUANTA 650 FEG SEM) operated at 5.5 kV and JEOL JSM-6300, whereas the atomic structure was performed by high resolution transmission electron microscopy (HRSEM/STEM) using a JEM-2200F equipment at 200 kV of accelerating voltage. The BET method applied in the nitrogen adsorption isotherms obtained from a Quantachrome Autosorb-3B apparatus was used to obtain the specific surface area, pore size distribution, and pore volume of the powders. Prior to the adsorption, the compounds were desorbed under high vacuum at 300°C during 3 hours. The surface chemical states of the compounds were analyzed by X-ray Photon Spectroscopy technique using a VG Escalab 220i XL spectrometer after exciting the samples by a nonmonochromatized Mg Kα line at 1253.6 eV. The band gap values of the ceramics were obtained using a spectrophotometer Varian Cary 100 UV-Vis.

2.3. Photocatalytic Evaluation. The photocatalytic activities of the composites were estimated by decomposition of 4-chlorophenol suspension at room temperature under visible light irradiation. The experimental procedure was realized following the same procedure previously reported [19].

3. Results and Discussion

Figure 1 shows XRD patterns of the sol-gel noble metal (Pt or Pd) doped TiO_2 catalysts using different molar percentages (1, 3, and 5) and calcined at 500°C. It can be seen that the undoped TiO_2 sample (Figures 1(a) and 1(b)) is featured by a combination of two structural phases, anatase and rutile. The diverse peaks match well with the crystallographic cards ICDD 89-4921 and ICDD 70-7347, for anatase and rutile structures, respectively. The XRD patterns for synthesized samples with 1 mol-% of Pd (Figure 1(a)) showed that palladium was almost totally incorporated into the anatase lattice where a weak peak of PdO was detected. At this composition is also evident that Pd addition at 1 mol-% caused an effect of stabilization for the anatase phase, inhibiting the formation of the rutile phase. The increment of Pd at 3 and 5 mol-% saturated the anatase lattice and as a consequence the PdO (ICCD 43-1024) and rutile phases were formed. In agreement with other works, the Pd addition enhances the anatase phase stabilization modifying the crystal growth [20]. However, such stabilization is misplaced after the saturation of the TiO_2 lattice in the anatase structure. On the other hand, Pt addition showed poor tendency to stabilize the anatase phase (Figure 1(b)). It can also observe the apparition of quite weak PtO_2 peaks (ICCD 73-2370), even with low amount of dopant [21]. These results point out that the Pt nanoparticles

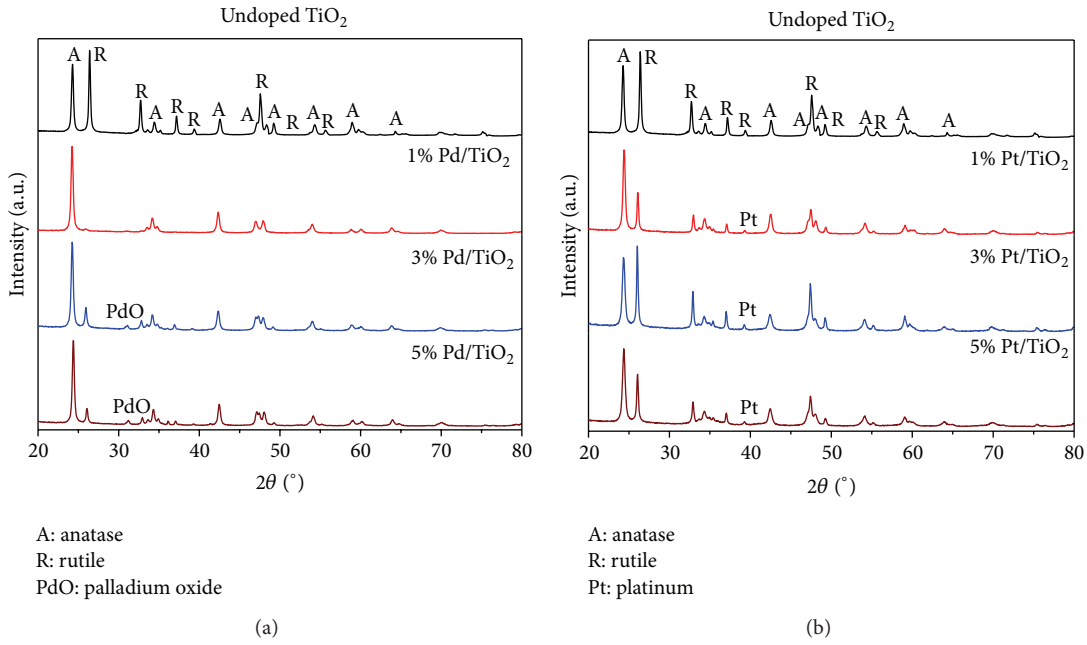

FIGURE 1: XRD patterns of undoped TiO_2 compared with (a) Pd/TiO_2 and (b) Pt/TiO_2 compounds.

could not be incorporated in the oxide matrix or interstitial sites; however, they led to obtaining catalysts with significant variation in the structure [22].

X-ray diffraction patterns were adjusted using Rietveld refinement to confirm and quantify the phases in the compounds. This method uses a theoretical structure modeling of the possible individual phases in the material to fit the whole powder diffraction pattern using a suitable analytical profile fitting function [23, 24]. It is important to consider crystallographic data (lattice parameters, fractional coordinates, occupancy, and temperature factor, etc.) of the diverse possible structures in the compounds as well as instrumental parameters [24]. However, estimating the volume contents of individual phases in a compound is a real challenge, due to the fact that multiphase materials could present partially or completely overlapped reflections [25]. The possible TiO_2 phases in the catalysts ($TiO_2(\beta)$, anatase, rutile, Pd, PdO, Pt, and PtO_2) were considered to fit the experimental profiles using the most suitable pseudo-Voigt analytical function [24, 26] modified with the Thompson-Cox-Hasting model. The quality of the Rietveld analysis is based on the R-factors (R_{wp}, R_{exp}, R_p), viewing graphically the observed and calculated patterns as well as ensuring that the model is chemically plausible [27–29]. The R_{wp} factor is the more valuable due to the fact that it does not depend on the absolute value of the intensities; but it depends on the background. In this sense, the weighted profile (R_{wp}) follows directly from the square root of the quantity minimized, scaled by the weighted intensities [27, 28]:

$$R_{wp} = \left[\frac{\sum w_i \left(y_{i(\text{obs})} - y_{i(\text{calc})} \right)^2}{\sum w_i \left(y_{i(\text{obs})} \right)^2} \right]^{1/2}, \quad (1)$$

where $y_{i(\text{obs})}$ is the observed intensity at the ith step, $y_{i(\text{calc})}$ is the calculated intensity at the ith step, and w_i is the weight. The best possible R_{wp} is called expected profile (R_{exp}). It reflects the quality of the obtained data in the measure of the XRD patterns (statically counts) [27, 28]:

$$R_{\text{exp}} = \left[\frac{(N - P)}{\sum w_i \left(y_{i(\text{obs})} \right)^2} \right]^{1/2}, \quad (2)$$

where N is the number of observed data, P is the number of parameters to refine, $y_{i(\text{obs})}$ is the observed intensity, and w_i is the weight. The average of these values is χ^2 or goodness of fit (GoF) [27–29]:

$$\chi^2 = \frac{R_{wp}}{R_{\text{exp}}}. \quad (3)$$

During the refinement process χ^2 starts out large when the model is poor and decreases as the model produces better agreement with the data [27]; when χ^2 is close to one, it can be considered that the values derived from least squares variance-covariance matrix are accurate. The results of the phase quantification of the as-prepared samples are summarized in Table 1. The diverse compounds displayed GoF values lower than 1.5 and graphically the observed and calculated patterns showed good fitting and minimum differences (Figures 2(a)–2(g)).

Thus, considering that R_{wp}, R_{exp}, and χ^2 have no statistical basis but are very valuable as a measure of refinement quality, we assume that a reasonable fitting was achieved [23, 27]. It is worth mentioning that the low values of GoF in the Rietveld refinement were considering the $TiO_2(\beta)$ phase in the analysis. $TiO_2(\beta)$ structure is usually obtained

Table 1: Percentages of phases determined and goodness of fit values (GoF) by Rietveld refinement.

Sample	Phase (vol-%)							R_{exp}	R_{wp}	R_p	GoF
	TiO_2(B) (B)	Anatase (A)	Rutile (R)	PdO	Pd	PtO_2	Pt				
Undoped TiO_2	1.37	29.40	69.23	—	—	—	—	4.64	6.90	5.43	1.49
1% Pd/TiO_2	2.86	92.65	3.87	0.63	—	—	—	4.72	5.43	4.18	1.15
3% Pd/TiO_2	2.42	71.39	25.00	1.14	0.05	—	—	4.51	5.71	4.39	1.27
5% Pd/TiO_2	1.59	77.51	19.51	1.25	0.14	—	—	4.57	5.28	4.00	1.15
1% Pt/TiO_2	—	67.05	32.8	—	—	—	0.15	4.01	5.15	3.91	1.28
3% Pt/TiO_2	1.87	48.03	49.55	—	—	0.18	0.37	4.56	5.85	4.54	1.28
5% Pt/TiO_2	2.07	59.11	37.70	—	—	0.11	1.01	4.39	5.10	3.93	1.16

at temperatures below 550°C [25, 27] and transforms into anatase phase with the temperature [6, 25, 30, 31]. The $TiO_2(\beta)$/anatase junction is free of stacking faults or defects and required a lowest energy pathway to transform into anatase which is a one-step transition; that is, their structures are related in nature [6]. These phases ($TiO_2(\beta)$ and anatase) are difficult to identify only by XRD technique because its reflections are in the 2θ range of 27–34° and 43–45° (ICCD 35-0088) showing non-well-defined peaks [19] as well as their close position with the rutile phase. Our previous studies [19] indicated that the synthesis conditions favored the $TiO_2(\beta)$ production explaining its residual content in the compounds (<3 vol-%). On the other hand, the Rietveld results of the 1% Pd/TiO_2 compound (Table 1) identified contributions of PdO phase in the XRD pattern. The low percentage of this phase (<1 vol-%) suggests that the majority of palladium was incorporated into the anatase lattice.

Rietveld refinement of Pd/TiO_2 and Pt/TiO_2 was used to obtain the anatase structure models and typical assemblies are shown in Figures 3(a)–3(c). For comparison, the Rietveld analysis of undoped TiO_2 structure is also showed in the figure. The structures of Pd-doped anatase phase (Figure 3(b)) and Pt-doped anatase phase (Figure 3(c)) showed variations in the lattice parameters and O-Ti-O bond distances compared with undoped anatase phase. These modifications suggest that Pd^{4+} and Pt^{4+} ions incorporate into the anatase structure, because Ti^{4+} (0.605 Å), Pd^{4+} (0.615 Å), and Pt^{4+} (0.625 Å) have similar ionic radii [32]. It is known that some dopants stabilize the anatase phase by occupying interstices, thereby distorting the anatase lattice and restricting the lattice contraction involved in the transformation to rutile [6]. Besides, the closer values of Ti^{4+} and Pd^{4+} ions could explain the higher amount of quantity of anatase phase in these compounds. Finally, it is possible to observe that anatase phase is present in all the specimens showing diverse combinations with other phases (since ~30 to ~93 vol-% content) which could result in materials with better photocatalytic properties [10–12].

An estimation of the crystal size was also obtained with Rietveld refinement and the results are shown in Figures 4(a)–4(c). From this figure, it seems that the crystal dimensions varied according to the structural phase. The highest crystal sizes were found for the undoped TiO_2 samples, ~67 nm for anatase and ~50 nm for rutile, whereas monoclinic beta-TiO_2 displays a value of ca. 5 nm. In general, except for this last structural phase, the crystal size of anatase and rutile reduces with the Pd or Pt addition (Figures 4(a) and 4(b)) in the range of 30–60 nm, approximately. This effect has been previously reported, indicating that metal ions doped titania provoked a reduction in the nucleation process [33]. Another feature to highlight in Figure 4(c) is that longer amounts of Pd provoke secondary phases formation (Pd and PdO) with an important crystal size (~232 nm); whilst independent of the quantity of Pt added to TiO_2, the crystallite size of the formed secondary phases are lower than 10 nm. The results pointed out that the synthesis parameters and preparation method more than noble metal content play a key role in the composition of structural phases and crystal sizes [34, 35].

Raman spectroscopy was used to characterize the formed phases in the Titania base catalysts (Figures 5(a) and 5(b)). All the Raman spectra present contributions at 153(E_g), 201(E_g), 403(B_{1g}), 525(B_{1g}), and 644(E_g) cm^{-1}, corresponding to the crystalline anatase phase [35, 36]. Raman peaks at 245 (2nd order), 450(E_g), and 617(A_{1g}) cm^{-1} are attributed to rutile crystal system [35, 36]. It can be noticed that spectra show a clear diminishing in all the bands which is generally correlated with the amount of dopants [37]. On the other hand, PdO signals (at ~663 cm^{-1}) were not identified in the TiO_2-Pd compounds, probably due to the overlap with rutile phase (650 cm^{-1}) [38]. In addition, expected Pt or PtO_2 signals were not observed due to the experimental setup limitations [39].

Figures 6(a)–6(i) display the morphology of the catalysts obtained by SEM and HRSEM techniques. The undoped TiO_2 compound (Figure 6(a)) contains irregular shape particles, which are aggregates of tiny crystals of TiO_2 phases [4]. The sizes observed in the noble metal doped TiO_2 samples match well with the crystallite size calculated from Rietveld analysis indicating that a good fitting was achieved. In general, it can be observed that Pt-doped samples displayed lower particle size than that presented by Pd-doped specimens. For example, 3% Pt/TiO_2 samples showed uniform Pt particles with sizes ~12 nm (Figure 6(c)), whereas 3% Pd/TiO_2 (Figure 6(b)) specimen exhibited agglomerates with variable diameter sizes between 15 and 400 nm; similar results were found with the other molar compositions (Figures 6(d)–6(i)). These results suggest that due to accepting species on the TiO_2 surface

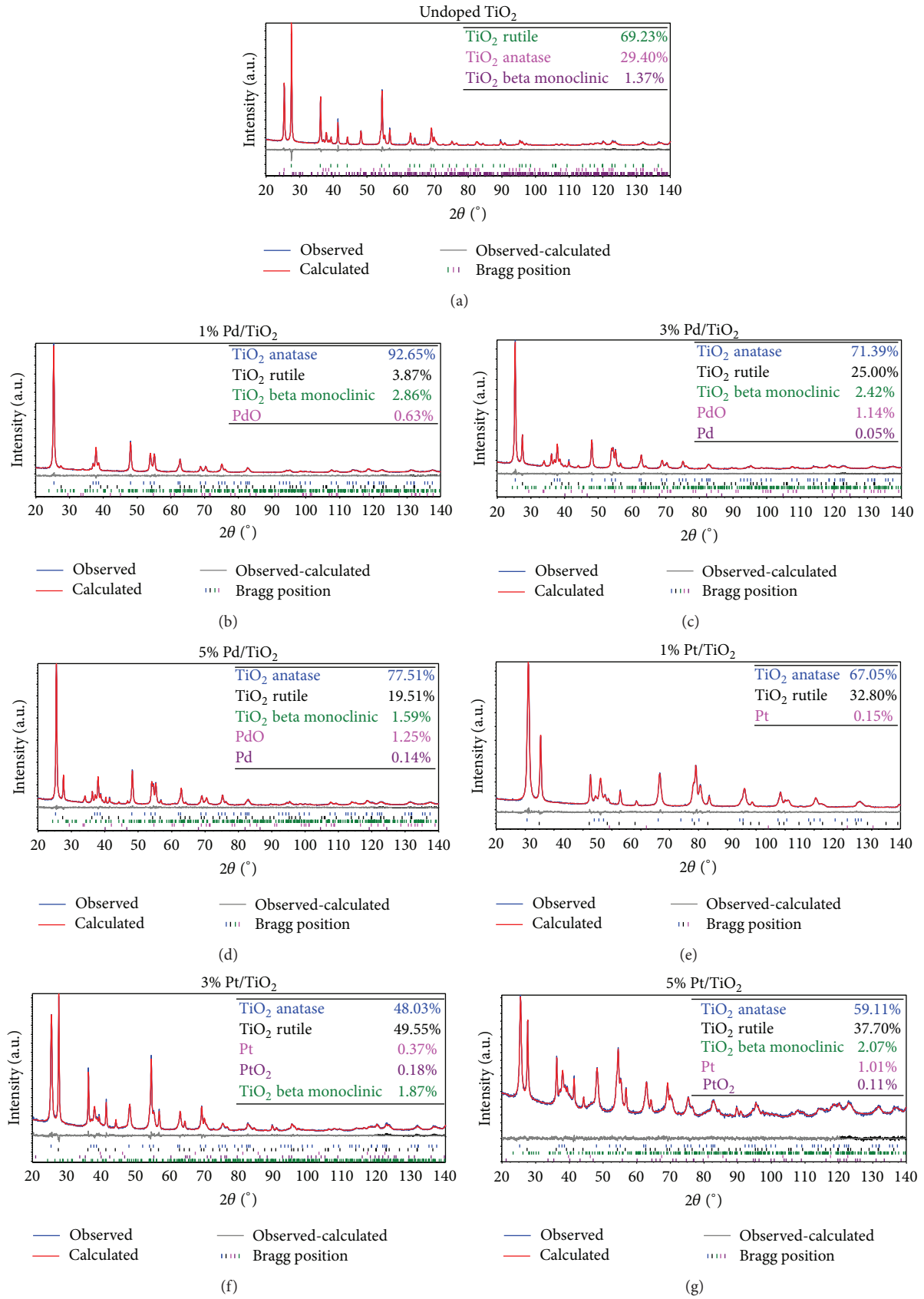

FIGURE 2: XRD of Rietveld refinement of (a) undoped TiO_2, (b) 1% Pd/TiO_2, (c) 3% Pd/TiO_2, (d) 5% Pd/TiO_2, (e) 1% Pt/TiO_2, (f) 3% Pt/TiO_2, and (g) 5% Pt/TiO_2 compounds thermally treated at 500°C.

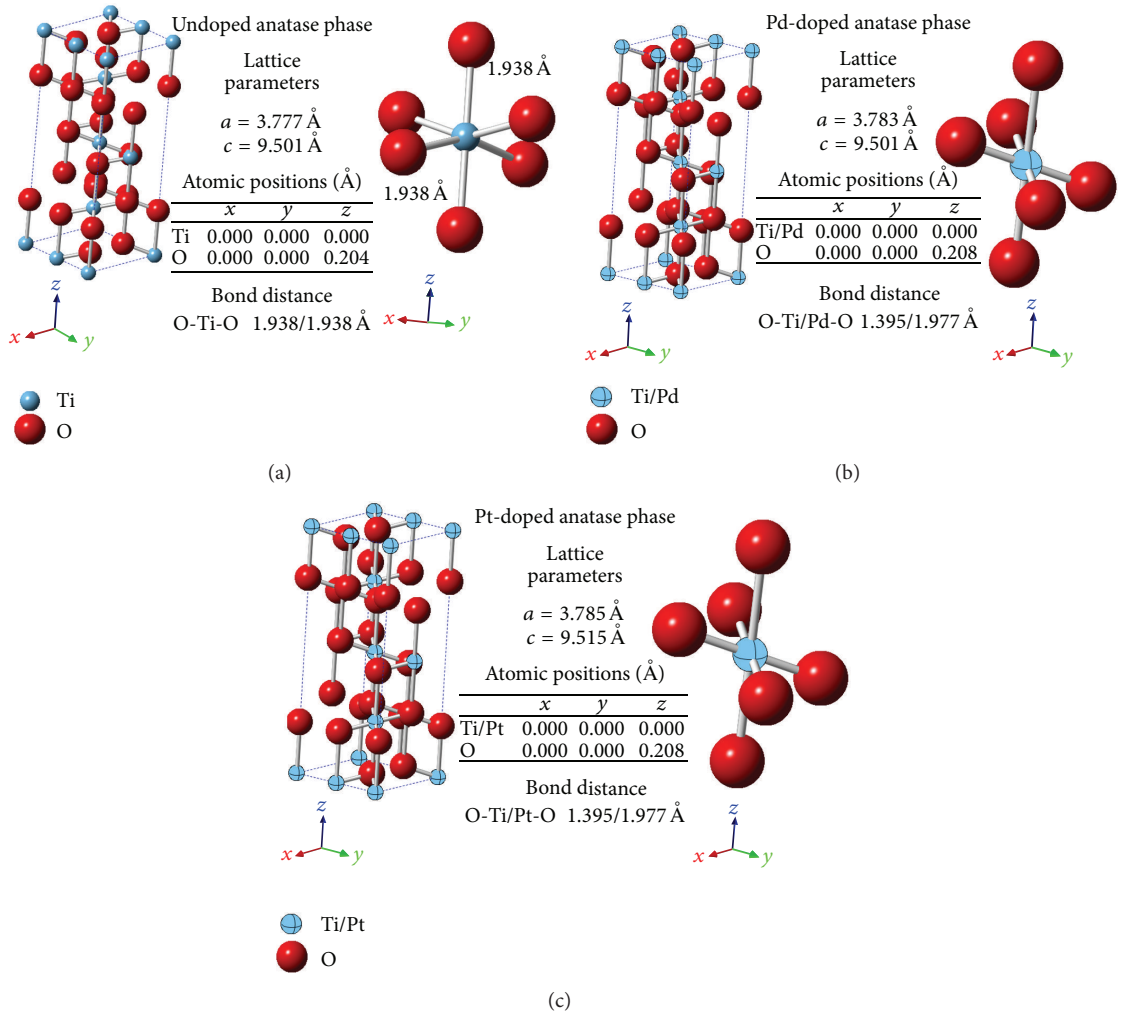

Figure 3: Representation of the structures obtained by Rietveld Refinement (a) undoped anatase phase, (b) Pd-doped anatase phase, and (c) Pt-doped anatase phase.

an enhancement on the electron-hole spatial separation can be expected, improving the photocatalytic properties of this material [4, 20].

HRTEM and STEM images of the as-prepared catalysts are shown in Figures 7(a)–7(l), where it is seen that undoped TiO_2 sample (Figures 7(a) and 7(b)) show crystalline and amorphous material [40]; 1% Pd/TiO_2 compound (Figure 7(c)) exhibits sharp and clear lattice fringes of anatase phase [20, 41]. Also, some nanoparticles of PdO (Figure 7(d)) are appreciated. In the 3% Pd/TiO_2 specimen PdO phase displayed sizes of around 15–20 nm (Figures 7(e) and 7(f)). The images of dark and bright field of the 5% Pd/TiO_2 (Figure 7(g) and 7(h)) displayed the crystals of the compounds. On the other hand, 1% Pt/TiO_2 (Figure 7(i)), 3% Pt/TiO_2 (Figures 7(k) and 7(j)), and 5% Pt/TiO_2 samples (Figure 7(i)) displayed Pt particles of around 4–14 nm with a semispherical shape [1]. It is important to highlight that the observed sizes in HRTEM are in agreement with the calculated sizes by Rietveld analysis.

Figure 8 presents adsorption-desorption isotherms obtained by the BET technique. Pd/TiO_2 (Figure 8(a)) and Pt/TiO_2 (Figure 8(b)) samples are compared with undoped TiO_2 compounds. All samples exhibit a type IV nitrogen isotherm due to the pore size measured (3.40 −3.71 nm), which is characteristic of mesoporous materials (Table 2). On the other hand, this kind of hysteresis loops is characteristic of solids consisting of aggregates (consolidated) or agglomerates (unconsolidated) of spherical particles and they correspond to the H_2 type because pores are nonuniform in size and shape [42]. It is important to mention that 3% Pd/TiO_2 catalyst presents very low values of surface area, which could be attributed to agglomerates in the samples previously observed in the HRSEM. In general, the surface areas obtained in these compounds are slightly low compared with other reports [43, 44].

XPS measurements were performed to determine impurities in the samples as well as to evaluate Pd and Pt content. Figures 9(a)–9(c) correspond to selected XPS survey spectra of undoped TiO_2, 3% Pd/TiO_2, and 3% Pt/TiO_2, respectively. In general, the spectra show two features assigned to Ti(IV) titanium in the IV oxidation state of the diverse titania phases [41, 45]. These peaks (Figure 9(d)) correspond to Ti2p states at BE = 458.8 eV ($Ti2p_{3/2}$) and BE = 464.7 eV ($Ti2p_{1/2}$). On

Table 2: BET results and band gap values of the different materials obtained in this study.

Sample	BET (m^2/g)	Pore volume (cm^3/g)	Pore size (nm)	Band gap (eV)
Undoped TiO_2	15.18	0.02	3.43	3.01
1% Pd/TiO_2	50.70	0.08	3.42	2.91
3% Pd/TiO_2	1.09	0.006	3.70	2.94
5% Pd/TiO_2	77.87	0.11	3.44	3.13
1% Pt/TiO_2	20.14	0.01	3.71	1.67*
3% Pt/TiO_2	63.07	0.09	3.40	2.90
5% Pt/TiO_2	63.74	0.08	3.40	2.22*

*The reliability of these TiO_2 band gap values could be compromised.

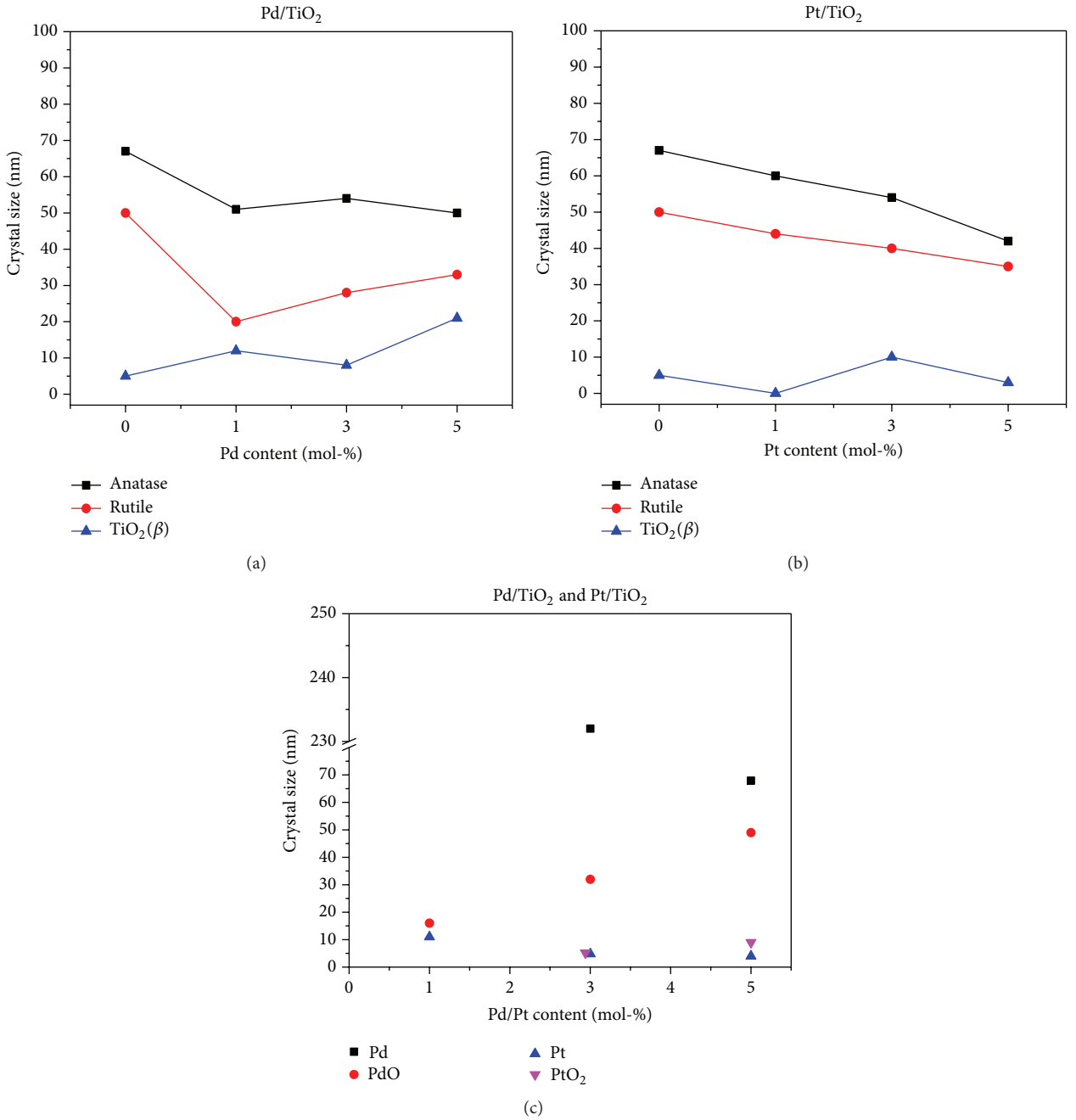

Figure 4: Crystal sizes estimated by Rietveld refinement of TiO_2 phases of (a) Pd/TiO_2 and (b) Pt/TiO_2 compounds as well as (c) crystal sizes of other phases formed.

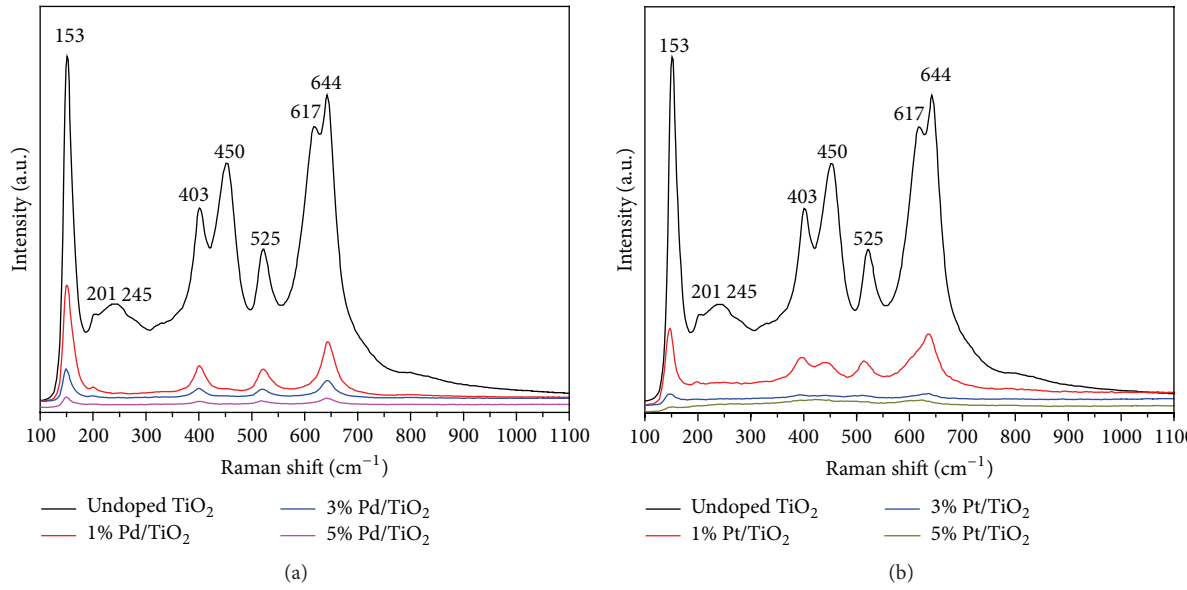

FIGURE 5: Raman spectra for undoped TiO_2 compared with (a) Pd/TiO_2 and (b) Pt/TiO_2 compounds.

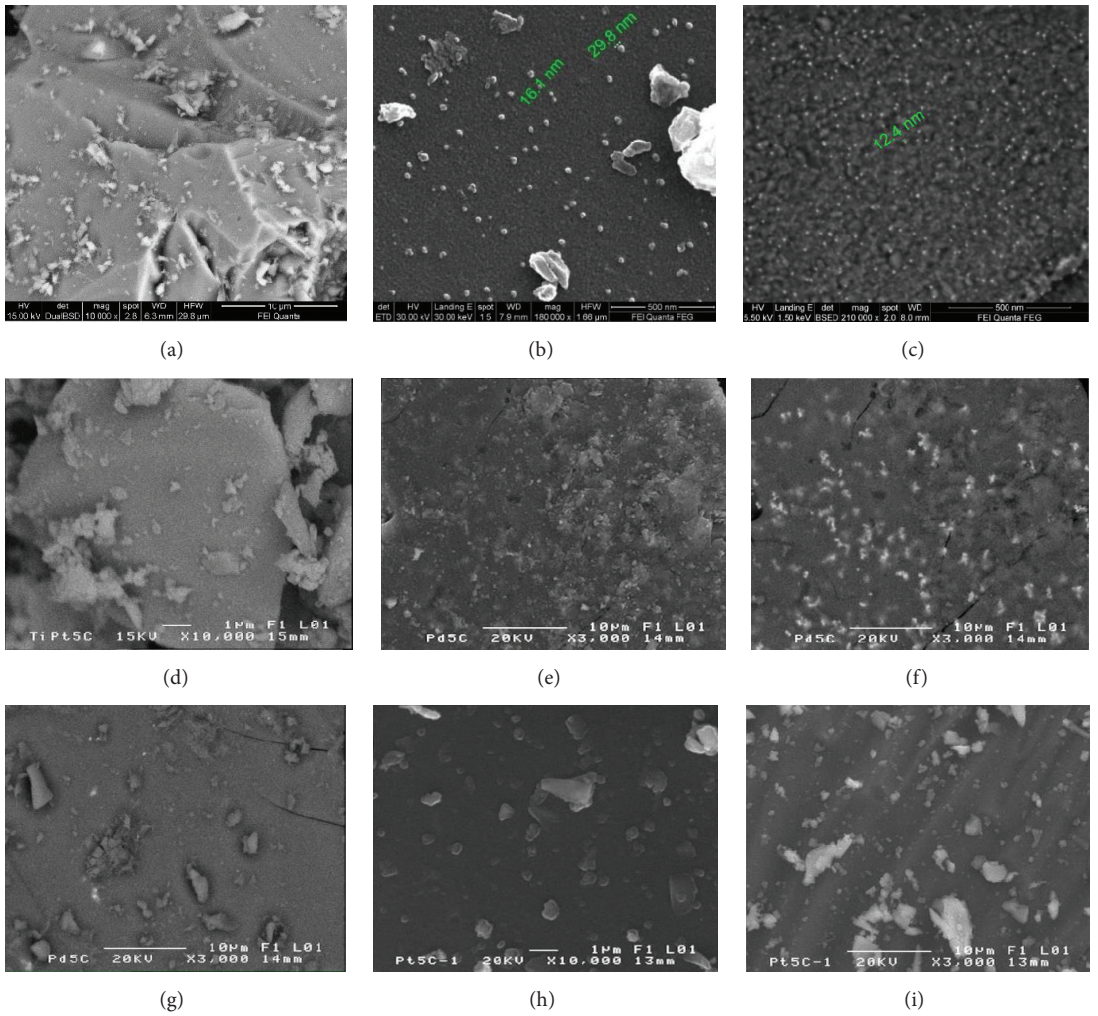

FIGURE 6: SEM and HRSEM micrographs of (a) undoped TiO_2, (b) 3% Pd/TiO_2, (c) 3% Pt/TiO_2, (d) 1% Pd/TiO_2, (e) 3% Pd/TiO_2, (f) 5% Pd/TiO_2, (g) 1% Pt/TiO_2, (h) 3% Pt/TiO_2, and (i) 5% Pt/TiO_2 samples.

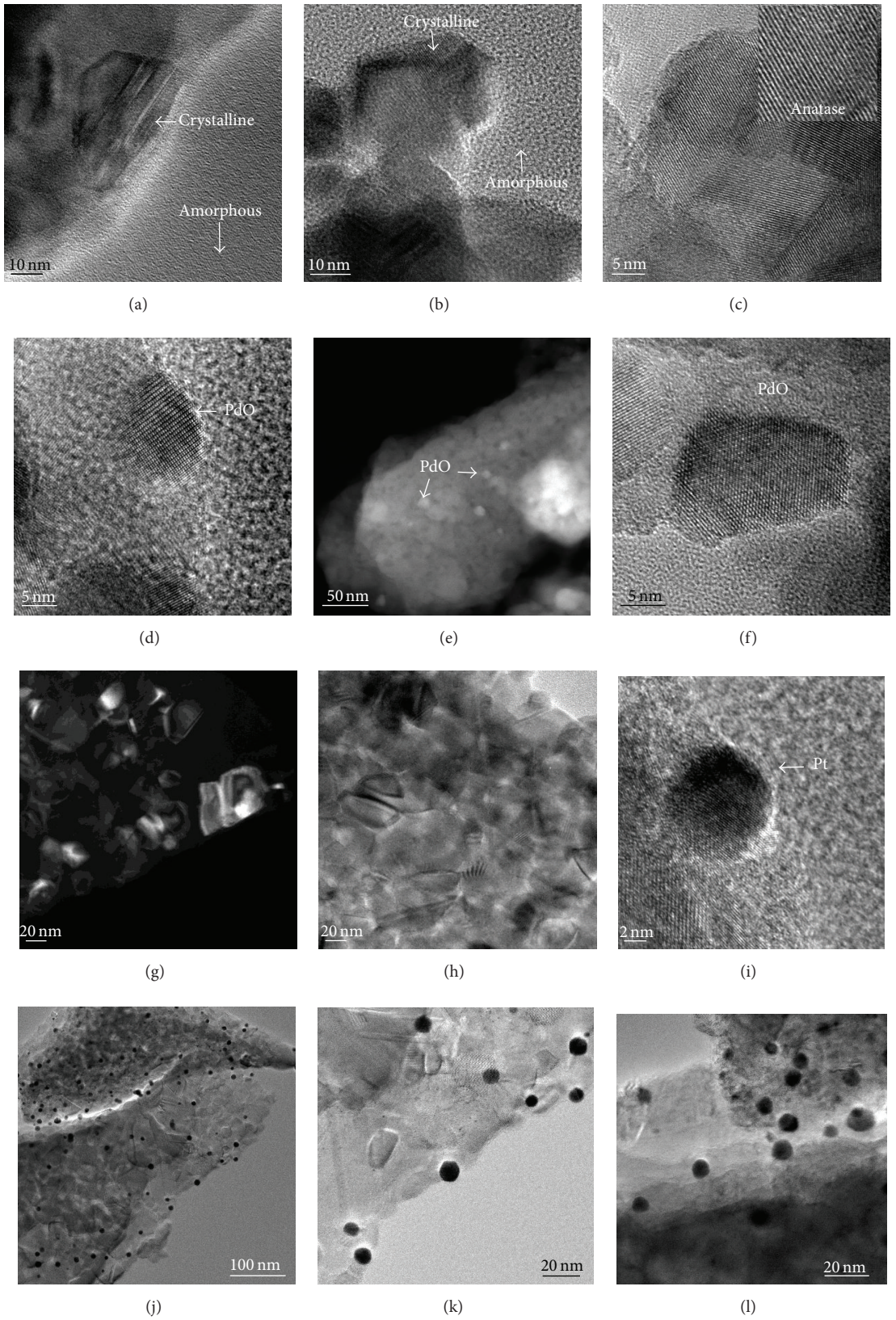

Figure 7: HRTEM and STEM images of (a) and (b) undoped TiO_2, (c) and (d) 1% Pd/TiO_2, (e) and (f) 3% Pd/TiO_2, (g) and (h) 5% Pd/TiO_2, (i) 1% Pt/TiO_2, (j) and (k) 3% Pt/TiO_2, and (l) 5% Pt/TiO_2 samples.

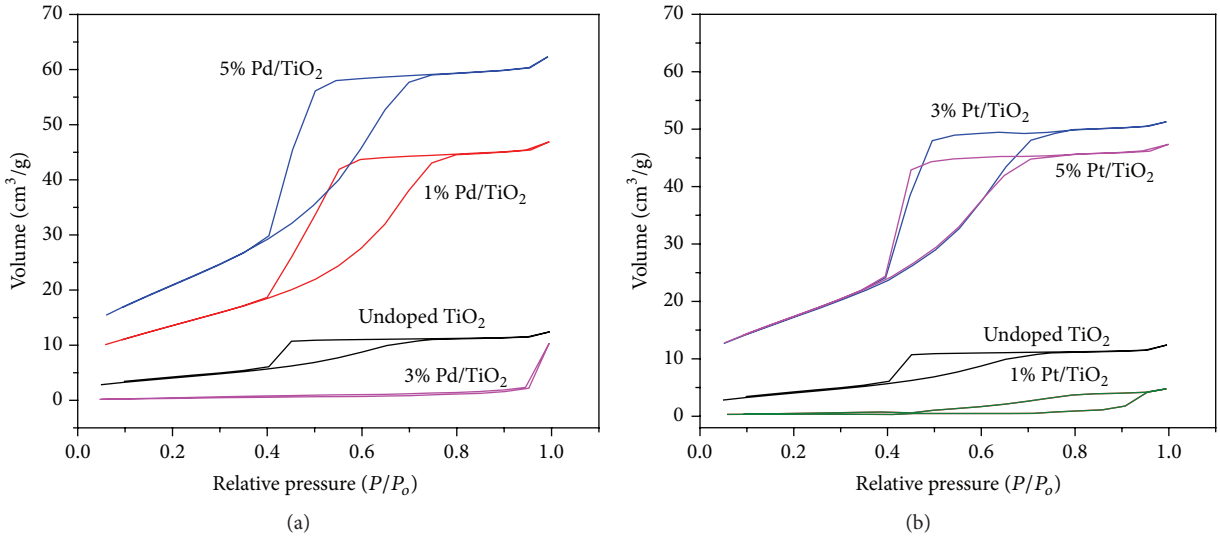

Figure 8: Adsorption/desorption isotherms of (a) Pd/TiO_2 and (b) Pt/TiO_2 catalysts in comparison with undoped TiO_2 compounds.

the other hand, the Pd signal is quite weak due to the fact that moderate counts were used in this sample; however, they were enough to relate the peak to the Pd3d state (Figure 9(e)) at 336 eV and it is a characteristic pointer of the PdO phase [46]. The typical XPS doublets peaks of 4f signal for Pt were observed at biding energies of 74.2 eV and 71.0 eV [47, 48]. Finally, a quantification of the elements is shown in Table 3, where it is seen the quantification of C, O, Ti, Pd, and Pt; thus, we assumed the obtaining of pure phases; however, it cannot discard the presence of small quantities of carbon impurities formed during sample preparation.

The 4-CP main absorption band at 278 nm was used to quantify the concentration of the pollutant in the solution using UV-vis measurements. Figures 10(a) and 10(b) present the degradation measurements of Pd/TiO_2 and Pt/TiO_2 compounds; both systems were compared with the undoped TiO_2 sample and the commercial Degussa P25. The photocatalysis process is based on the energy transfer through the interaction of an excited semiconductor and (in this case) an aqueous solution. This interface generates a local density of charge (electron-hole) that produces an electric field promoting the charge transfer. In this sense, diverse reactions could be produced in the catalyst surface; however, the efficiency in the degradation rate of pollutant is influenced by the active site and the photoabsorption of the catalyst used [49]. In this work, it is clear that all the synthesized compounds showed better response than the commercial Degussa P25 that started to degrade until 75 min later. This could be attributed to the photocatalytic activity of titanium dioxide because it is greatly influenced by the crystalline form [38, 50] and the combinations of phases between catalysts are different. The best results correspond to 1% Pd/TiO_2 catalyst which eliminates the pollutant almost 8 times faster after 105 min. Apparently, Pd addition provoked the transference of photogenerated electrons from TiO_2 conduction band to the dopant conduction and the holes were accumulated in the TiO_2 valence band reducing electron-hole

Table 3: Quantification by XPS technique.

Sample	Atomic%				
	C	O	Ti	Pd	Pt
Undoped TiO_2	26.6	52.2	21.2	—	—
3% Pd/TiO_2	21.4	55.4	23.0	0.2	—
3% Pt/TiO_2	21.9	54.5	22.4	—	1.2

pair recombination [4, 51], thus improving the photocatalytic activity. On the other hand, with the increment of Pd content we expected an enhancement in the photocatalytic response; however, 3% Pd/TiO_2 and 5% Pd/TiO_2 catalysts suffered a slight decrement in the degradation efficiency (~90%), possibly due to the excess of PdO that masked the TiO_2 surface and reduced the light absorption capability [49]. One of the most active metals for photocatalytic enhancement is platinum (Pt) and the capture of electrons by this metal is postulated to produce longer electron-hole pair separation, lifetime hindering the electron-hole pairs recombination and enhancing the transfer of holes and possibly electrons to O_2 adsorbed on the TiO_2 surface [18]. However, in this work, the photocatalytic effect of Pt/TiO_2 compounds was slightly different compared with Pd/TiO_2 compounds; nevertheless, our results show a better degradation performance in comparison with the commercial one. Also, even the compounds with Pt content at 3 mol-% and 5 mol-% eliminate 7 times faster the pollutant. From the different compounds evaluated the more efficient catalyst was the one with major content of anatase phase (~92 vol-%), in agreement with the literature [49, 52].

It is worth mentioning that the catalysts show good degradation efficiency at UV light exposure; however, to complement this information it is necessary to know the band gap to determine if these compounds could work under visible light. The catalysts were characterized by reflectance measurements. Figure 11 presents a large absorption band between 1.54 and 3.0 eV (400–800 nm) due to

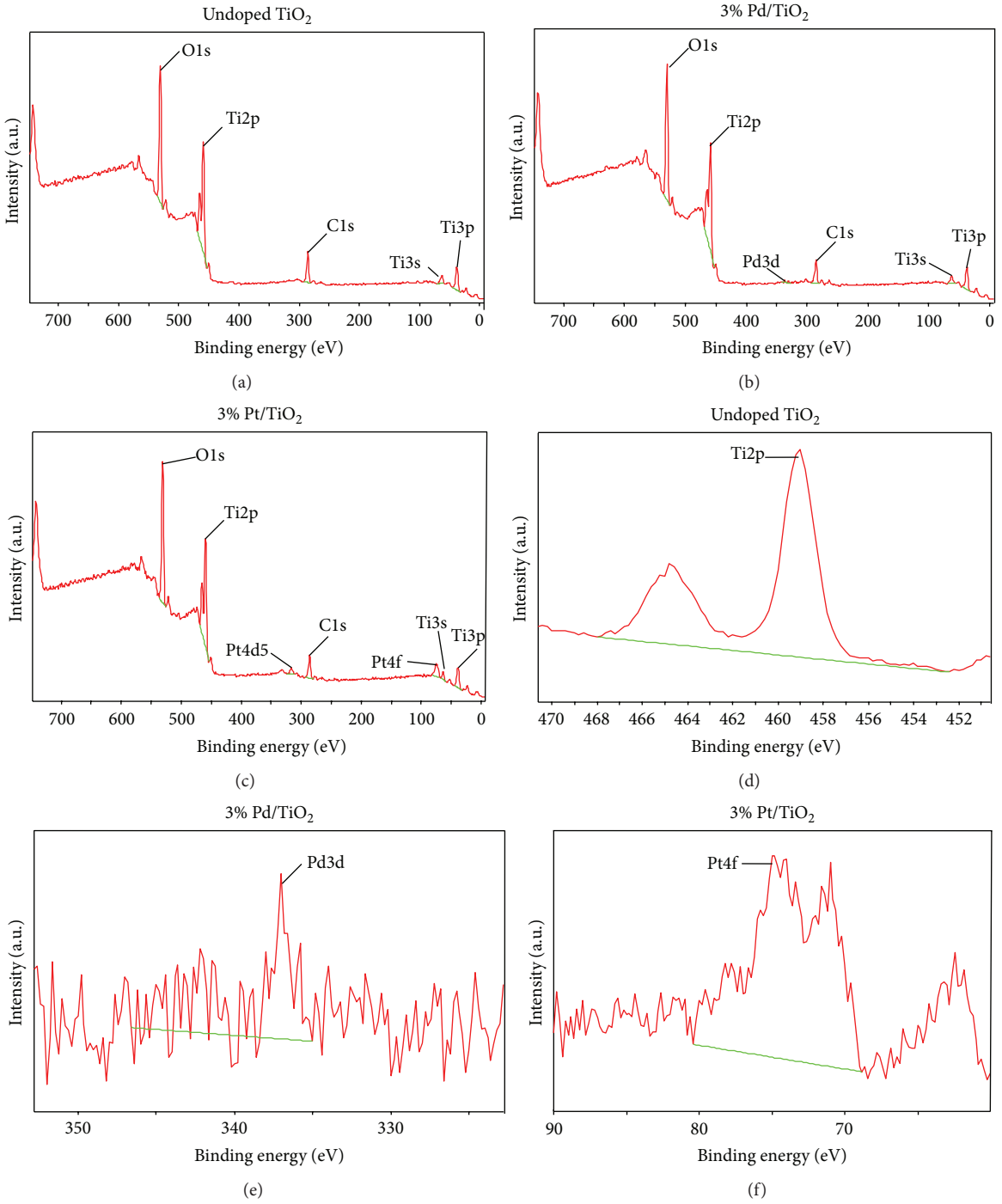

Figure 9: XPS spectra for of (a) undoped TiO_2, (b) 3% Pd/TiO_2, and (c) 3% Pt/TiO_2 catalyst.

the $O^{2-}(2p) \rightarrow Ti^{4+}(3d)$ transitions in the tetrahedral symmetry [53, 54] as well as contributions of the noble metals; however, the TiO_2 absorption spectrum was not substantially modified allowing to estimate the band gap, through Kubelka-Munk (K-M or $F(R)$) function [55] based on

$$F(R) = \frac{(1-R)^2}{2R}, \tag{4}$$

where R is the reflectance and $F(R)$ is proportional to the extinction coefficient (α) [55–57]. A modified $F(R)$ function can be obtained by multiplying the function by $h\nu$, where h is Planck's constant and ν is the light frequency (s^{-1}) using the corresponding coefficient ($n = 1/2$, for indirect allowed transitions) associated with an electronic transition as follows:

$$(F(R) * h\nu)^n. \tag{5}$$

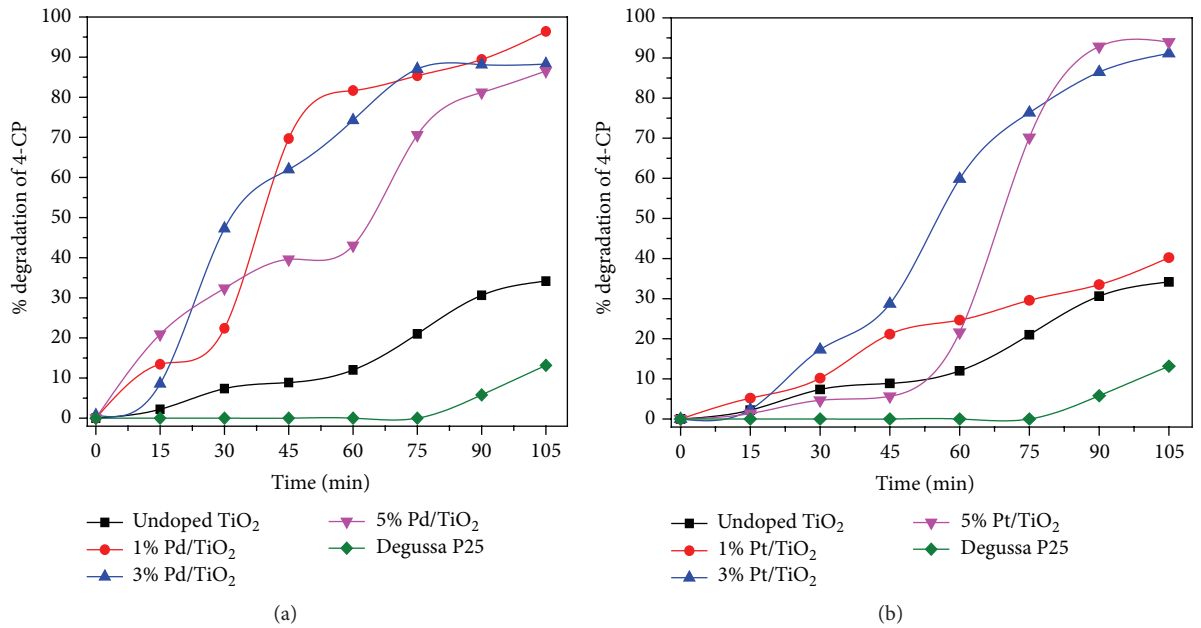

FIGURE 10: Photodegradation percentages of 4-CP using (a) Pd/TiO_2 and (b) Pt/TiO_2 catalysts. Both systems were compared with undoped TiO_2 and commercial Degussa P25 compounds.

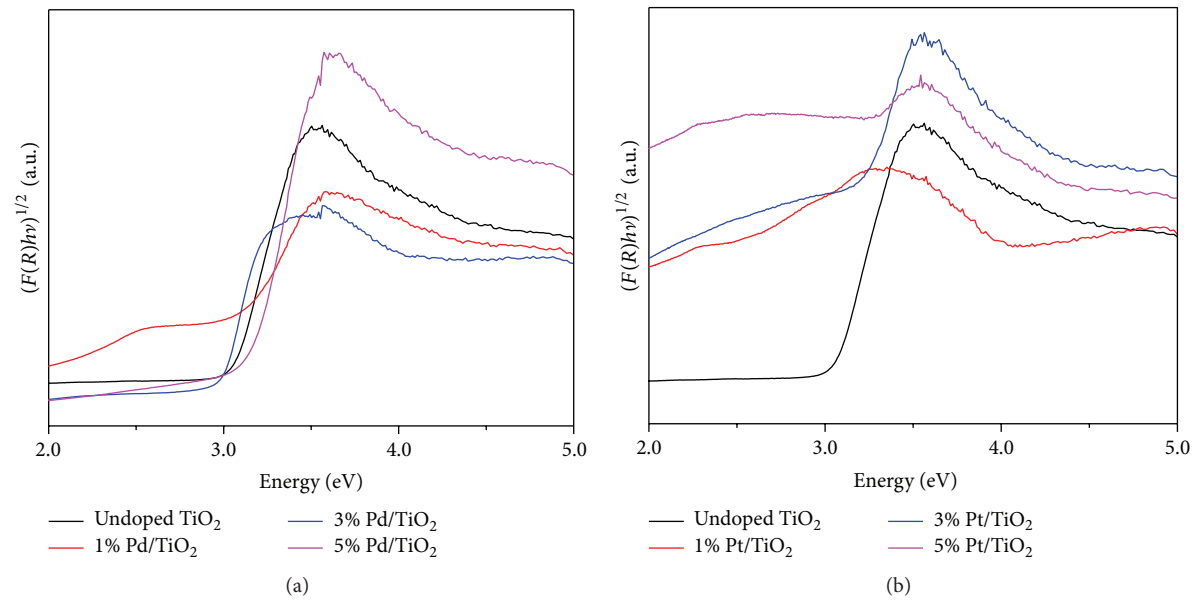

FIGURE 11: UV-vis spectra of the undoped TiO_2 compared with (b) Pd/TiO_2 and Pt/TiO_2 compounds.

By plotting this equation as a function of the energy in eV, the band gap (E_g) of semiconductor particles can be obtained [37], whereas for practical purposes, the band gap energy for the different samples can be calculated using the following equation:

$$E_g = \frac{1239.84 * m}{-b}. \quad (6)$$

In this equation, m and b are obtained by the linear fit ($y = mx+b$) of the flat section of the UV-vis spectrum [57]. Table 2 presents the obtained band gaps of the compounds. Undoped TiO_2 sample exhibits a band gap value of 3.01 eV, lower value than the commercial Degussa P25 (3.16–3.18) [58, 59]. On the other hand, with addition of the dopant (Pd and Pt) E_g value shifts up to 1.67 eV. The reduction of the band gaps could be attributed to additional levels of the Ti3d conduction band formed in the TiO_2 [20]. These results point out that these catalysts could also work under other frequencies of the electromagnetic spectrum extending their applications; however, more experiments need to be realized.

These results show that engineering TiO_2 catalysts by a mix of different phases is a research axis of considerable interest, because it enhances the photocatalytic behavior compared with single-phase titania. The sol-gel route has been widely used to synthesize TiO_2 compounds and many researches have been developed about this area. Nevertheless, the route of synthesis followed in this work favored to control the kinetics anatase-rutile phase transformation corroborating the importance of the effect processing conditions to modify crystalline size, grain size, surface area, and morphology as well as phase distribution [31]. The synthesized compounds were compared with Degussa P-25, one commercial photocatalyst which is utilized as a reference material in many studies and all the compounds showed better photocatalytic behavior attributed to the Schottky barrier-type charge separation from the deposition of noble metals on TiO_2.

4. Conclusions

In summary, undoped TiO_2, Pd/TiO_2, and Pt/TiO_2 catalysts with diverse structural compositions were successfully synthesized using sol-gel method. XRD and RAMAN results indicate that Pd and Pt addition achieved modifying the anatase-rutile transformation obtaining diverse catalysts with a combination of phases. Rietveld analysis revealed the vol-% content of anatase (from ~30 to ~93 vol-%) in the catalysts as well as its combination with other phases. HRTEM confirmed the formation of anatase phase and the nanometric size of the catalysts. HRSEM displayed the good distribution of the dopants in the samples. All the compounds showed better response in the degradation of 4-chlorophenol (almost eight times faster in the case of Pd/TiO_2 at 1 mol-%) than the commercial Degussa P25, though their efficiency depends on the Schottky barrier-type separation from the deposition of noble metals on TiO_2. The results obtained here show that the photoactivity of TiO_2 was enhanced notwithstanding the low value of surface area. The arrangement of phases as well as the Pd and Pt doping induced a blue shift in the band gap energy, which explains the observed catalytic behavior of the samples. Finally, these results are very promising for the use of this type of catalysts in the elimination of other pollutants under other frequencies of the electromagnetic spectrum extending their applications.

Competing Interests

The authors declare that they have no competing interests.

Acknowledgments

The authors are thankful to Dr. Javier Arturo Montes de Oca Valero (RIP.) for his unvalued support in the realization of this research. D. S. García-Zaleta is grateful for his postgraduate fellowship to CONACYT and SIP-IPN. The authors want to acknowledge Andres De Luna for the proofreading and the Universidad Juárez Autónoma de Tabasco for the given support.

References

[1] C. B. Molina, A. H. Pizarro, J. A. Casas, and J. J. Rodriguez, "Aqueous-phase hydrodechlorination of chlorophenols with pillared clays-supported Pt, Pd and Rh catalysts," *Applied Catalysis B: Environmental*, vol. 148-149, pp. 330–338, 2014.

[2] M. J. Morra, V. Borek, and J. Koolpe, "Transformation of chlorinated hydrocarbons using aquocobalamin or coenzyme F430 in combination with zero-valent iron," *Journal of Environmental Quality*, vol. 29, no. 3, pp. 706–715, 2000.

[3] A. Ayati, A. Ahmadpour, F. F. Bamoharram, B. Tanhaei, M. Mänttäri, and M. Sillanpää, "A review on catalytic applications of Au/TiO_2 nanoparticles in the removal of water pollutant," *Chemosphere*, vol. 107, pp. 163–174, 2014.

[4] S. Sakthivel, M. V. Shankar, M. Palanichamy, B. Arabindoo, D. W. Bahnemann, and V. Murugesan, "Enhancement of photocatalytic activity by metal deposition: characterisation and photonic efficiency of Pt, Au and Pd deposited on TiO_2 catalyst," *Water Research*, vol. 38, no. 13, pp. 3001–3008, 2004.

[5] Y. Hu, H.-L. Tsai, and C.-L. Huang, "Phase transformation of precipitated TiO_2 nanoparticles," *Materials Science and Engineering A*, vol. 344, no. 1-2, pp. 209–214, 2003.

[6] J. F. Banfield, D. R. Veblen, and D. J. Smith, "The identification of naturally occurring TiO_2(B) by structure determination using high-resolution electron microscopy, image simulation, and distance-least-squares refinement," *American Mineralogist*, vol. 76, no. 3-4, pp. 343–353, 1991.

[7] Q. Zhang, L. Gao, and J. Guo, "Effects of calcination on the photocatalytic properties of nanosized TiO_2 powders prepared by $TiCl_4$ hydrolysis," *Applied Catalysis B: Environmental*, vol. 26, no. 3, pp. 207–215, 2000.

[8] T. Ohno, K. Sarukawa, and M. Matsumura, "Photocatalytic activities of pure rutile particles isolated from TiO_2 powder by dissolving the anatase component in HF solution," *The Journal of Physical Chemistry B*, vol. 105, no. 12, pp. 2417–2420, 2001.

[9] A. Zielińska-Jurek and J. Hupka, "Preparation and characterization of Pt/Pd-modified titanium dioxide nanoparticles for visible light irradiation," *Catalysis Today*, vol. 230, pp. 181–187, 2014.

[10] H.-F. Yu and S.-T. Yang, "Enhancing thermal stability and photocatalytic activity of anatase-TiO_2 nanoparticles by co-doping P and Si elements," *Journal of Alloys and Compounds*, vol. 492, no. 1-2, pp. 695–700, 2010.

[11] K. Naeem and F. Ouyang, "Preparation of Fe^{3+}-doped TiO_2nanoparticles and its photocatalytic activity under UV light," *Physica B: Condensed Matter*, vol. 405, no. 1, pp. 221–226, 2010.

[12] R. R. Bacsa and J. Kiwi, "Effect of rutile phase on the photocatalytic properties of nanocrystalline titania during the degradation of p-coumaric acid," *Applied Catalysis B: Environmental*, vol. 16, no. 1, pp. 19–29, 1998.

[13] H. Jiang, Q. Wang, S. Zang, J. Li, and Q. Wang, "Enhanced photoactivity of Sm, N, P-tridoped anatase-TiO_2 nano-photocatalyst for 4-chlorophenol degradation under sunlight irradiation," *Journal of Hazardous Materials*, vol. 261, pp. 44–54, 2013.

[14] Q. Wang, H. Jiang, S. Zang, J. Li, and Q. Wang, "Gd, C, N and P quaternary doped anatase-TiO_2 nano-photocatalyst for enhanced photocatalytic degradation of 4-chlorophenol under simulated sunlight irradiation," *Journal of Alloys and Compounds*, vol. 586, pp. 411–419, 2014.

[15] M. N. Chong, B. Jin, C. W. K. Chow, and C. Saint, "Recent developments in photocatalytic water treatment technology: a review," *Water Research*, vol. 44, no. 10, pp. 2997–3027, 2010.

[16] E. Antonlini, "Palladum in fuel cell catalysis," *Energy & Environmental Science*, vol. 2, pp. 915–931, 2009.

[17] J. Kua and W. A. Goddard III, "Oxidation of methanol on 2nd and 3rd row group VIII transition metals (Pt, Ir, Os, Pd, Rh, and Ru): application to direct methanol fuel cells," *Journal of the American Chemical Society*, vol. 121, no. 47, pp. 10928–10941, 1999.

[18] H.-W. Chen, Y. Ku, and Y.-L. Kuo, "Effect of Pt/TiO_2 characteristics on temporal behavior of o-cresol decomposition by visible light-induced photocatalysis," *Water Research*, vol. 41, no. 10, pp. 2069–2078, 2007.

[19] D. S. García-Zaleta, J. A. Montes de Oca-Valero, A. M. Torres-Huerta et al., "Effect of Pd addition on the nanostructure and properties of Pd/TiO_2 catalysts for the photocatalytic degradation of 4-chlorophenol," *Journal of Nano Research*, vol. 28, pp. 9–20, 2014.

[20] Z. Wu, Z. Sheng, H. Wang, and Y. Liu, "Relationship between Pd oxidation states on TiO_2 and the photocatalytic oxidation behaviors of nitric oxide," *Chemosphere*, vol. 77, no. 2, pp. 264–268, 2009.

[21] Z. Rui, S. Wu, C. Peng, and H. Ji, "Comparison of TiO_2 Degussa P25 with anatase and rutile crystalline phases for methane combustion," *Chemical Engineering Journal*, vol. 243, pp. 254–264, 2014.

[22] A. V. Rosario and E. C. Pereira, "The role of Pt addition on the photocatalytic activity of TiO_2 nanoparticles: the limit between doping and metallization," *Applied Catalysis B: Environmental*, vol. 144, pp. 840–845, 2014.

[23] H. M. Rietveld, "Line profiles of neutron powder-diffraction peaks for structure refinement," *Acta Crystallographica*, vol. 22, no. 1, pp. 151–152, 1967.

[24] R. A. Young and D. B. Wiles, "Profile shape functions in Rietveld refinements," *Journal of Applied Crystallography*, vol. 15, no. 4, pp. 430–438, 1982.

[25] L. Brohan, A. Verbaere, M. Tournoux, and G. Demazeau, "La transformation TiO_2(B)-anatase," *Materials Research Bulletin*, vol. 17, no. 3, pp. 355–361, 1982.

[26] P. Bose, S. K. Pradhan, and S. Sen, "Rietveld analysis of polymorphic transformations of ball milled anatase TiO_2," *Materials Chemistry and Physics*, vol. 80, no. 1, pp. 73–81, 2003.

[27] B. H. Toby, "R factors in Rietveld analysis: how good is good enough?" *Powder Diffraction*, vol. 21, no. 1, pp. 67–70, 2006.

[28] R. A. Young, *The Rietveld Method. International Union Crystallography*, Science Publications, Oxford, UK, 1995.

[29] L. B. Mccusker, R. B. Von Dreele, D. E. Cox, D. Louër, and P. Scardi, "Rietveld refinement guidelines," *Journal of Applied Crystallography*, vol. 32, no. 1, pp. 36–50, 1999.

[30] A. Orendorz, A. Brodyanski, J. Lösch et al., "Phase transformation and particle growth in nanocrystalline anatase TiO_2 films analyzed by X-ray diffraction and Raman spectroscopy," *Surface Science*, vol. 601, no. 18, pp. 4390–4394, 2007.

[31] H.-L. Kuo, C.-Y. Kuo, C.-H. Liu, J.-H. Chao, and C.-H. Lin, "A highly active bi-crystalline photocatalyst consisting of TiO_2 (B) nanotube and anatase particle for producing H_2 gas from neat ethanol," *Catalysis Letters*, vol. 113, no. 1-2, pp. 7–12, 2007.

[32] R. D. Shannon, "Revised effective ionic radii and systematic studies of interatomic distances in halides and chalcogenides," *Acta Crystallographica Section A*, vol. 32, no. 5, pp. 751–767, 1976.

[33] D. A. H. Hanaor and C. C. Sorrell, "Review of the anatase to rutile phase transformation," *Journal of Materials Science*, vol. 46, no. 4, pp. 855–874, 2011.

[34] K. Suttiponparnit, V. Tiwari, M. Sahu, P. Biswas, S. Suvachittanont, and T. Charinpanitkul, "Effect of Pt or Pd doping on stability of TiO_2 nanoparticle suspension in water," *Journal of Industrial and Engineering Chemistry*, vol. 19, no. 1, pp. 150–156, 2013.

[35] L. Kernazhitsky, V. Shymanovska, T. Gavrilko et al., "Room temperature photoluminescence of anatase and rutile TiO_2 powders," *Journal of Luminescence*, vol. 146, pp. 199–204, 2014.

[36] A. S. Bolokang, D. E. Motaung, C. J. Arendse, and T. F. G. Muller, "Morphology and structural development of reduced anatase-TiO_2 by pure Ti powder upon annealing and nitridation: Synthesis of TiO_x and TiO_xN_y powders," *Materials Characterization*, vol. 100, pp. 41–49, 2015.

[37] R. López and R. Gómez, "Photocatalytic degradation of 4-nitrophenol on well characterized sol-gel molybdenum doped titania semiconductors," *Topics in Catalysis*, vol. 54, no. 8-9, pp. 504–511, 2011.

[38] H. Lee, M. Shin, M. Lee, and Y. J. Hwang, "Photo-oxidation activities on Pd-doped TiO_2 nanoparticles: critical PdO formation effect," *Applied Catalysis B: Environmental*, vol. 165, pp. 20–26, 2015.

[39] A. Lahmar, N. Pfeiffer, S. Habouti, and M. Es-Souni, "Microstructure and property control in TiO_2-Pt nanocomposite thin films," *Ceramics International*, vol. 41, no. 1, pp. 443–449, 2014.

[40] M. Abdul Khadar and N. A. Mohemmed Shanid, "Nanoscale fine-structure evaluation of RF magnetron sputtered anatase films using HRTEM, AFM, micro-Raman spectroscopy and fractal analysis," *Surface and Coatings Technology*, vol. 204, no. 9-10, pp. 1366–1374, 2010.

[41] J. Zhang, L. Qian, L. Yang et al., "Nanoscale anatase TiO_2 with dominant {111} facets shows high photocatalytic activity," *Applied Surface Science*, vol. 311, pp. 521–528, 2014.

[42] G. Leofanti, M. Padovan, G. Tozzola, and B. Venturelli, "Surface area and pore texture of catalysts," *Catalysis Today*, vol. 41, no. 1–3, pp. 207–219, 1998.

[43] O. Mekasuwandumrong, S. Phothakwanpracha, B. Jongsomjit, A. Shotipruk, and J. Panpranot, "Influence of flame conditions on the dispersion of Pd on the flame spray-derived Pd/TiO_2 nanoparticles," *Powder Technology*, vol. 210, no. 3, pp. 328–331, 2011.

[44] G. L. Chiarello, M. V. Dozzi, M. Scavini, J.-D. Grunwaldt, and E. Selli, "One step flame-made fluorinated Pt/TiO_2 photocatalysts for hydrogen production," *Applied Catalysis B: Environmental*, vol. 160-161, no. 1, pp. 144–151, 2014.

[45] Y. Liu, H. Wang, H. Li et al., "Length-controlled synthesis of oriented single-crystal rutile TiO_2 nanowire arrays," *Journal of Colloid and Interface Science*, vol. 363, no. 2, pp. 504–510, 2011.

[46] K. Kočí, L. Matějová, M. Reli et al., "Sol-gel derived Pd supported TiO_2-ZrO_2 and TiO_2 photocatalysts; their examination in photocatalytic reduction of carbon dioxide," *Catalysis Today*, vol. 230, pp. 20–26, 2014.

[47] B. Ruiz-Camacho, M. A. Valenzuela, R. G. González-Huerta, K. Suarez-Alcantara, S. E. Canton, and F. Pola-Albores, "Electrochemical and XAS investigation of oxygen reduction reaction on Pt-TiO_2-C catalysts," *International Journal of Hydrogen Energy*, vol. 38, no. 28, pp. 12648–12656, 2013.

[48] C. Encarnación Gómez, J. R. Vargas García, J. A. Toledo Antonio, M. A. Cortes Jacome, and C. Ángeles Chávez, "Pt

nanoparticles on titania nanotubes prepared by vapor-phase impregnation-decomposition method," *Journal of Alloys and Compounds*, vol. 495, no. 2, pp. 458–461, 2010.

[49] L. M. Pastrana-Martínez, S. Morales-Torres, A. G. Kontos et al., "TiO_2, surface modified TiO_2 and graphene oxide-TiO_2 photocatalysts for degradation of water pollutants under near-UV/Vis and visible light," *Chemical Engineering Journal*, vol. 224, no. 1, pp. 17–23, 2013.

[50] G. S. Pozan and A. Kambur, "Significant enhancement of photocatalytic activity over bifunctional ZnO-TiO_2 catalysts for 4-chlorophenol degradation," *Chemosphere*, vol. 105, pp. 152–159, 2014.

[51] C.-C. Tsai and H. Teng, "Structural features of nanotubes synthesized from NaOH treatment on TiO_2 with different post-treatments," *Chemistry of Materials*, vol. 18, no. 2, pp. 367–373, 2006.

[52] M. Hussain, R. Ceccarelli, D. L. Marchisio, D. Fino, N. Russo, and F. Geobaldo, "Synthesis, characterization, and photocatalytic application of novel TiO_2 nanoparticles," *Chemical Engineering Journal*, vol. 157, no. 1, pp. 45–51, 2010.

[53] R. López, R. Gómez, and M. E. Llanos, "Photophysical and photocatalytic properties of nanosized copper-doped titania sol-gel catalysts," *Catalysis Today*, vol. 148, no. 1-2, pp. 103–108, 2010.

[54] J. Chen, L.-B. Lin, and F.-Q. Jing, "Theoretical study of F-type color center in rutile TiO_2," *Journal of Physics and Chemistry of Solids*, vol. 62, no. 7, pp. 1257–1262, 2001.

[55] P. Kubelka and F. Munk, "Ein beitrag zur optik der farbanstriche," *Zeitschrift fuer Technische Physik*, vol. 12, pp. 593–601, 1931.

[56] R. López and R. Gómez, "Band-gap energy estimation from diffuse reflectance measurements on sol-gel and commercial TiO_2: a comparative study," *Journal of Sol-Gel Science and Technology*, vol. 61, no. 1, pp. 1–7, 2012.

[57] P. Kubelka, "New contributions to the optics of intensely light-scattering materials. Part I," *Journal of the Optical Society of America*, vol. 38, pp. 448–457, 1948.

[58] G.-M. Zuo, Z.-X. Cheng, H. Chen, G.-W. Li, and T. Miao, "Study on photocatalytic degradation of several volatile organic compounds," *Journal of Hazardous Materials*, vol. 128, no. 2-3, pp. 158–163, 2006.

[59] M. A. Behnajady and H. Eskandarloo, "Silver and copper co-impregnated onto TiO_2-P25 nanoparticles and its photocatalytic activity," *Chemical Engineering Journal*, vol. 228, pp. 1207–1213, 2013.